This is a repository copy of *Thin GaAsSb diodes with low excess noise*.

White Rose Research Online URL for this paper:
https://eprints.whiterose.ac.uk/119042/

Version: Published Version

Article:
Zhou, X., Pinel, L. orcid.org/0000-0001-8603-5631, Dimler, S. et al. (3 more authors) (2017) Thin GaAsSb diodes with low excess noise. IEEE Journal of Selected Topics in Quantum Electronics, 24 (2). 3800105. pp. 1-5. ISSN 1077-260X

https://doi.org/10.1109/JSTQE.2017.2725441

Reuse
This article is distributed under the terms of the Creative Commons Attribution (CC BY) licence. This licence allows you to distribute, remix, tweak, and build upon the work, even commercially, as long as you credit the authors for the original work. More information and the full terms of the licence here: https://creativecommons.org/licenses/

Takedown
If you consider content in White Rose Research Online to be in breach of UK law, please notify us by emailing eprints@whiterose.ac.uk including the URL of the record and the reason for the withdrawal request.

eprints@whiterose.ac.uk
https://eprints.whiterose.ac.uk/

Thin $Al_{1-x}Ga_xAs_{0.56}Sb_{0.44}$ Diodes With Low Excess Noise

Xinxin Zhou, Lucas L. G. Pinel, Simon J. Dimler, Shiyong Zhang, Jo Shien Ng, *Member, IEEE*, and Chee Hing Tan, *Member, IEEE*

***Abstract*—Thin avalanche layers have been adopted to achieve low excess noise and high-gain bandwidth products in InP and InAlAs avalanche photodiodes. In this paper, we report the excess noise characterization in a series of $Al_{1-x}Ga_xAs_{0.56}Sb_{0.44}$ ($x = 0, 0.05, 0.1, 0.15$) diodes with avalanche layer thickness of 110–116 nm. These alloys, lattice matched to InP, showed lower excess noise than InP and InAlAs. Dark current, most probably originating from surface leakage, was observed to be lower in composition with higher Ga concentration. Avalanche gain and excess noise measurements using lasers of 543 and 633 nm wavelengths indicated that at a given electric field, the electron ionization coefficient is larger than the hole ionization coefficient. Using the 543 nm laser, low excess noise data corresponding to an effective ionization coefficient ratio of $k = 0.1$ in the conventional excess noise theory was measured in $Al_{1-x}Ga_xAs_{0.56}Sb_{0.44}$ ($x = 0.05$, 0.1, 0.15), although pure electron injection was not achieved. Our results demonstrated the potential of using $Al_{1-x}Ga_xAs_{0.56}Sb_{0.44}$ ($x = 0.05, 0.1, 0.15$) as replacement for InP and InAlAs for high speed and low excess noise avalanche photodiodes. The data reported in this paper is available from the ORDA digital repository (https://doi.org/10.15131/shef.data.5155822).**

***Index Terms*—Avalanche photodiodes, impact ionization, noise measurement.**

I. Introduction

HIGH-SPEED avalanche photodiodes (APDs) are key components in long-haul high bit rate optical communication systems because they exploit internal gain to provide higher sensitivity than a conventional p^+in^+ photodiode. However, in most semiconductors, the inherently stochastic impact ionization process produces excess noise, which can degrade the signal-to-noise ratio of the detection system. Low excess noise and high gain-bandwidth product (GBP) are therefore crucial for achieving high bit rate optical communication systems.

The classical McIntyre model [1] shows that materials with low ionization coefficient ratio, *k*, are required to achieve low excess noise. Therefore early APDs with thick avalanche layers and operated at low electric fields, where *k* tends to be low, could achieve low excess noise. On the other hand, to maximise the gain-bandwidth product, the narrowest possible avalanche region should be employed [2]. As the avalanche region is narrowed to increase the APD's gain-bandwidth product, excess noise was expected to increase, because the narrow APDs operated with higher electric fields, where *k* tends to unity. In practice, however, low excess noise was measured from narrow avalanche regions [3], [4], which was eventually attributed to the increased significance of carrier dead space as the avalanche region narrows [5], [6]. Therefore APDs are now designed with narrow avalanche regions to achieve high GBP and low excess noise simultaneously. Nevertheless, there remains a lower limit of avalanche layer thickness imposed by the onset of band-to-band tunnelling current: ~180 nm for InP and 150 nm for InAlAs avalanche regions, respectively [7].

Commercial APDs that combine an InGaAs absorption region with an InP or InAlAs avalanche region are used in optical communication systems operating at bit rates up to 10 Gb/s. However, due a low GBP that is typically 80-140 GHz [8], [9], an InGaAs/InP APD does not have sufficient bandwidth with appreciable gain at bit rates above 10 Gb/s. Higher GBPs, up to 240–270 GHz [10], [11] were achieved using InGaAs/InAlAs APDs with ~100 nm avalanche region and small APD diameter (e.g. 14 μm in [10]) to avoid significant tunneling current. Although even higher GBP (340 GHz) was demonstrated by Ge/Si APDs, with Si avalanche region and Ge absorption region [12], their dark current and quantum efficiency are not comparable to those of InGaAs/InP or InGaAs/InAlAs APDs. Hence researchers continue to investigate other materials as alternative avalanche layer materials. A promising candidate is GaSb/AlInAsSb APD, which can be grown latticed-matched to GaSb substrates. Highly desirable excess noise characteristics were reported in [13].

Recently $AlAs_{0.56}Sb_{0.44}$ (hereafter referred to as AlAsSb) lattice-matched to an InP substrate, was reported as an alternative avalanche material for 1310 and 1550 nm wavelength APDs. It offers very good thermal stability (<1 mV/K temperature coefficient of the avalanche breakdown voltage [14]) and very low excess noise factor [15]. The smallest effective *k* (0.05)

Manuscript received June 1, 2017; revised June 29, 2017 and June 30, 2017; accepted July 4, 2017. This work was supported in part by the UK Engineering and Physical Sciences Research Council (EP/K001469/1) and in part by the European Union H2020 Program (PROMIS, under Grant H2020-MSCA-ITN-2014-641899). *(Corresponding author: Lucas L. G. Pinel.)*

X. Zhou was with the Department of Electronic and Electrical Engineering, University of Sheffield, Sheffield S3 7HQ, U.K. She is now with the Oclaro Technology, Ltd., Towchester NN12 8EQ, U.K. (e-mail: xinxin.zhou@oclaro.com).

L. Pinel, S. J. Dimler, J. S. Ng, and C. H. Tan are with the Department of Electronic and Electrical Engineering, University of Sheffield, Sheffield S3 7HQ, U.K. (e-mail: l.pinel@sheffield.ac.uk; s.dimler@sheffield.ac.uk; j.s.ng@sheffield.ac.uk; c.h.tan@sheffield.ac.uk).

S. Zhang is with the EPSRC National Epitaxy Facility, University of Sheffield, Sheffield S3 7HQ, U.K. (e-mail: Shiyong.Zhang@sheffield.ac.uk).

Color versions of one or more of the figures in this paper are available online at http://ieeexplore.ieee.org.

Digital Object Identifier 10.1109/JSTQE.2017.2725441

This work is licensed under a Creative Commons Attribution 3.0 License. For more information, see http://creativecommons.org/licenses/by/3.0/

TABLE I
STRUCTURE DETAILS OF THE $Al_{1-x}Ga_xAs_{0.56}Sb_{0.44}$ WAFERS USED

Layer	Material	Thickness (nm)
p^+ (Be-doped)	$In_{0.53}Ga_{0.47}As$	100
p^+ (Be-doped)	$Al_{1-x}Ga_xAs_{0.56}Sb_{0.44}$	300
i	$Al_{1-x}Ga_xAs_{0.56}Sb_{0.44}$	111 ($x = 0$) 116 ($x = 0.05$) 114 ($x = 0.10$) 110 ($x = 0.15$)
n^+ (Si-doped)	$Al_{1-x}Ga_xAs_{0.56}Sb_{0.44}$	100
n^+ (Si-doped)	$In_{0.53}Ga_{0.47}As$	1000
n^+ InP substrate		

was measured from a 230 nm AlAsSb avalanche region [15], which improves on the effective *k* of 0.09 from Ge/Si APDs [12]. However, the surface leakage current in these AlAsSb APDs was not completely suppressed.

A more recent study on $Al_{1-x}Ga_xAs_{0.56}Sb_{0.44}$ ($x = 0, 0.05, 0.1, 0.15$) showed that incorporating Ga into $AlAs_{0.56}Sb_{0.44}$ could substantially reduce surface leakage current [16]. As the Ga content, *x*, increases from 0 to 0.15, the surface leakage current at 90% of the breakdown voltage was reduced by almost two orders of magnitude. The corresponding temperature coefficient of breakdown remains desirably low, ranging from 0.86 to 1.08 $mV{\cdot}K^{-1}$ [16]. Having also demonstrated a high GBP of 424 GHz with an InGaAs/$Al_{1-x}Ga_xAs_{0.56}Sb_{0.44}$ APD for 1550 nm wavelength light [17], excess noise factors and ionization coefficients of the alloy $Al_{1-x}Ga_xAs_{0.56}Sb_{0.44}$ are the remaining APD-related characteristics that have not been investigated. In this work, we report experimental work on excess noise on thin $Al_{1-x}Ga_xAs_{0.56}Sb_{0.44}$ ($x = 0, 0.05, 0.10, 0.15$) diodes with nominal 100 nm avalanche regions, which are relevant to high-speed APDs.

II. EXPERIMENTAL DETAILS

The $Al_{1-x}Ga_xAs_{0.56}Sb_{0.44}$ ($x = 0, 0.05, 0.10, 0.15$) p^+in^+ wafers used for this work are identical to those used in [16]. Structures of the four wafers, all grown on n^+ InP substrates by molecular beam epitaxy, are summarized in Table I. Each wafer has an $Al_{1-x}Ga_xAs_{0.56}Sb_{0.44}$ *i*-region, with width, *w*, of 100 nm sandwiched between a p^+ and an n^+ $Al_{1-x}Ga_xAs_{0.56}Sb_{0.44}$ cladding layer. Top and bottom highly doped $In_{0.53}Ga_{0.47}As$ contact layers at either side were included to facilitate good ohmic contacts. Wafer pieces were fabricated into circular mesa diodes with diameters of 50, 100, 200 and 400 μm, by standard photolithography and wet chemical etching. The mixtures were citric acid: H_2O_2 (ratio of 2: 1) for InGaAs and HCl: H_2O_2: de-ionised water (ratio of 5:1:50) for Al(Ga)AsSb. Ti-Au was deposited to form the metal contacts of the diodes. The diodes had no anti-reflection coating or dielectric passivation.

Characterization of the diodes began with dark Current–Voltage (*I-V*) characteristics under reverse bias to ensure the diodes were sufficiently robust for subsequent measurements. Capacitance-Voltage (*C-V*) characteristics were measured from the fabricated diodes and were corroborated by secondary ion mass spectroscopy on as-grown wafer pieces (details in [16]). From these, *i*-region thicknesses from 110 to 116 nm, also listed in Table I, for the four wafers were deduced. *C-V* characteristics were also recorded to facilitate subsequent excess noise factor versus avalanche gain, *F*(*M*), measurements.

The *F*(*M*) measurements were carried out using the experimental setup and procedure described in [3]. In this work continuous-wave He-Ne lasers, with emission wavelengths of 543 and 633 nm, were the light sources used to generate photocurrent in the device-under-test (DUT). These lasers offered light that can be absorbed by the devices of this work, whilst having sufficiently stable light output level to facilitate *F*(*M*) measurements. The laser light was mechanically modulated at $\sim$180 Hz before being focused into an optical spot within the optical window of the device-under-test (DUT). Care was taken to ensure that light is well confined within the optical window to avoid generation of photocarriers at the edge of devices. The resultant photocurrent and noise power were measured simultaneously as functions of reverse bias by two lock-in amplifiers (model SR830). For a given reverse bias, *V*, multiplication, *M,* was given by the ratio of measured photocurrent to the injected photocurrent. The latter was estimated from measured photocurrent values at small reverse bias, while taking into account the increase of injected photocurrent with reverse bias due to widening of the depletion region [18], to avoid overestimating the avalanche gain.

For a given set of *M* versus *V*, *F* was given by the ratio of the measured noise power to the predicted shot noise power. Accuracy of the predicted shot noise power required the DUT's *C-V* characteristics. Also, the shot noise power versus photocurrent characteristics of the two lasers used were measured and were found to be low compared to the measured multiplied noise power when DUT was in place. The *F*(*M*) experimental setup yields more accurate results when the capacitance of the DUT is $<$30 pF, hence the *F*(*M*) measurements focused on devices with nominal radius of either 50 or 100 μm (see Fig. 1). For a given wafer and a given laser wavelength, between 5-10 devices were tested to obtain *M*(*V*) and *F*(*M*). Mean and standard deviation of *M* and *F* were then deduced for each wafer to enable data comparison between different wafers.

The different laser wavelengths produced different carrier injection profiles within the DUT. As the light enters the device, light of either wavelength is strongly absorbed by the 100 nm p^+ InGaAs cap layer [19]. However carriers generated by photon absorption within this InGaAs layer are unlikely to contribute to the photocurrent, due to the large InGaAs/AlGaAsSb conduction band offsets. The reported large conduction band offset between InGaAs and AlAsSb ranges from 1.6 [20] to 1.74 eV [21]. Although the bandgaps of AlGaAsSb [16] are smaller than that of AlAsSb, the conduction band offsets between InGaAs/AlGaAsSb are likely to remain.

Considering only the light remaining after the p^+ InGaAs cap layer, it is necessary to estimate the percentage of light absorbed in the 300 nm thick p^+ $Al_{1-x}Ga_xAs_{0.56}Sb_{0.44}$ cladding

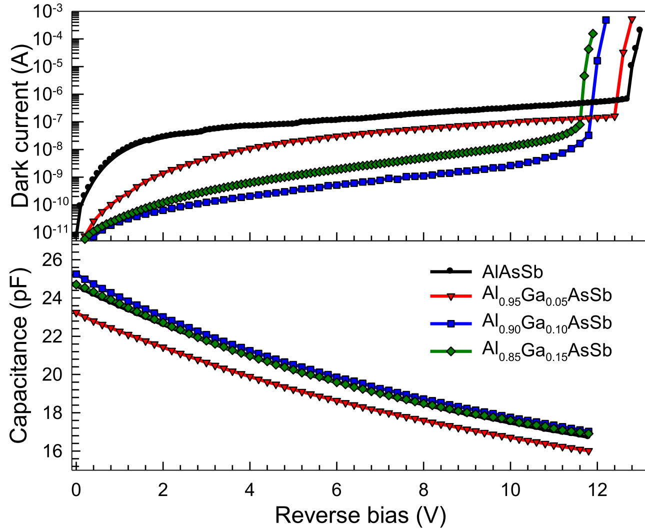

Fig. 1. Typical room temperature reverse dark *I-V* (top) and *C-V* (bottom) for 100 μm radii devices of the $Al_{1-x}Ga_xAs_{0.56}Sb_{0.44}$ wafers.

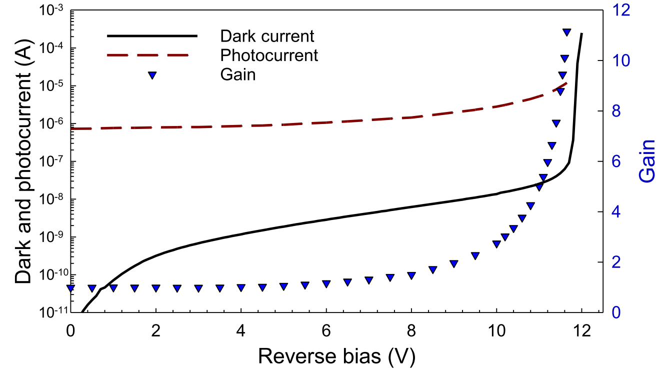

Fig. 2. Example of dark current, photocurrent, and avalanche gain versus reverse bias from the *F*(*M*) measurements. Data shown are from the $Al_{1-x}Ga_xAs_{0.56}Sb_{0.44}$ wafer.

TABLE II
ESTIMATED $AL_{1-x}GA_xAS_{0.56}SB_{0.44}$ ABSORPTION COEFFICIENTS AND PERCENTAGE OF LIGHT ABSORBED BY THE p^+ - $AL_{1-x}GA_xAS_{0.56}SB_{0.44}$ CLADDING LAYER

	Absorption coefficient (cm^{-1})		Percentage of light absorbed by 300 nm of $Al_{1-x}Ga_xAs_{0.56}Sb_{0.44}$ (%)	
	543 nm	633 nm	543 nm	633 nm
$x = 0$	2.5×10^4	3.6×10^2	53	1
$x = 0.05$	3.6×10^4	5.9×10^3	66	16
$x = 0.10$	4.7×10^4	1.1×10^4	76	29
$x = 0.15$	5.8×10^4	1.7×10^4	82	40

layer. Absorption coefficients of $Al_{1-x}Ga_xAs_{0.56}Sb_{0.44}$ at 543 and 633 nm wavelength were estimated by interpolating absorption coefficients of four binary materials, AlAs [22], AlSb [23], GaAs [24], and GaSb [24]. Table II shows the estimated absorption coefficients and percentage of light absorbed in the p^+ $Al_{1-x}Ga_xAs_{0.56}Sb_{0.44}$ cladding layer. A combination of small absorption coefficient and thin p^+ $Al_{1-x}Ga_xAs_{0.56}Sb_{0.44}$ cladding layer resulted in carrier injection profiles with significant photogenerated carriers in the *i*-region and n^+ $Al_{1-x}Ga_xAs_{0.56}Sb_{0.44}$ cladding layer, as indicated by the percentage of light remaining after the p^+ $Al_{1-x}Ga_xAs_{0.56}Sb_{0.44}$ cladding layer. Consequently pure electron injection was not achieved. However, since a shorter wavelength light is absorbed more strongly, the 543 nm light gives a carrier injection profile that more closely resembles pure electron injection than the profile from the 633 nm light.

III. RESULTS AND DISCUSSION

Typical data of room temperature reverse dark *I-V* and *C-V* from 100 μm radius devices of the four wafers are shown in Fig. 1. The *I-V* data shows an abrupt increase in current with reverse bias at $\sim$ 12 V. When the Ga composition increases from 0 to 0.15, the breakdown voltage decreases slightly from 13.02 to 12.05 V, in line with the slight reduction in estimated bandgap energy from 1.64 to 1.56 eV [16]. For a given wafer, the value of reverse bias at which the abrupt increase occurs does not vary from device to device, nor is it affected by radius of the device. The dark current is believed to be predominantly surface leakage current as the dark currents do not scale with device area. For example, at 0.9 V_b, devices from the $Al_{1-x}Ga_xAs_{0.56}Sb_{0.44}$ wafer exhibit increasing dark current densities with decreasing device diameter (20, 60, 80, and 200 μA·cm^{-2} for device diameter of 200, 100, 50 and 25 μm, respectively). As the Ga composition increases, a clear drop in the dark current was observed. A more detailed temperature dependence of dark current in these devices has been reported in [25]. The dark current density of $\sim 5 \times 10^{-6}$ A/ cm^2 was measured at a bias voltage corresponding to 95% of the breakdown voltage at room temperature. This dark current density is 3 times lower than InP and 5 times lower than InAlAs avalanche layers of similar thicknesses, suggesting insignificant band to band tunnelling current in these thin $Al_{1-x}Ga_xAs_{0.56}Sb_{0.44}$ ($x = 0$ to 0.15). The measured capacitance is <30 pF, confirming the devices are suitable for excess noise measurements.

Examples of experimental dark current, photocurrent, and avalanche gain versus reverse bias obtained from the $Al_{1-x}Ga_xAs_{0.56}Sb_{0.44}$ wafer during *F*(*M*) measurements are shown in Fig. 2. Data of avalanche gain versus reverse bias obtained from *F*(*M*) measurements on the four wafers are shown in Fig. 3. To show differences between avalanche gain values at low gain values, the data are plotted as *M*-1 in a logarithmic scale. Uncertainty associated with estimating the injected photocurrent as a function of reverse bias resulted in unavoidable, large relative uncertainties for the individual set of small avalanche gain values. However, by using mean values from multiple devices for each wafer, the avalanche gain uncertainties are minimized. Avalanche gain increases rapidly as the reverse bias approaches $\sim$12 V, confirming that the abrupt increase in dark *I-V* observed in Fig. 1 is caused by avalanche breakdown, a bulk breakdown mechanism. Observing Fig. 3, in all wafers, for a given reverse bias, *M* increases when the laser wavelength decreases, i.e. when the carrier injection profile approaches pure electron injection with fewer electron-hole pairs generated in

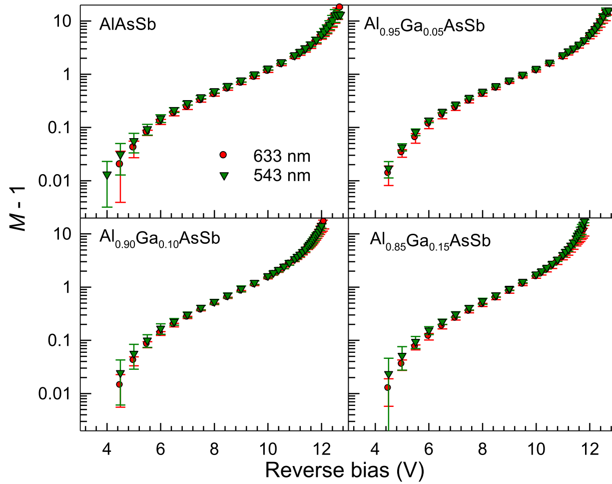

Fig. 3. Avalanche gain measured versus reverse bias for the $Al_{1-x}Ga_xAs_{0.56}Sb_{0.44}$ diodes using 633 nm (•) and 543 nm (▼) wavelength lasers.

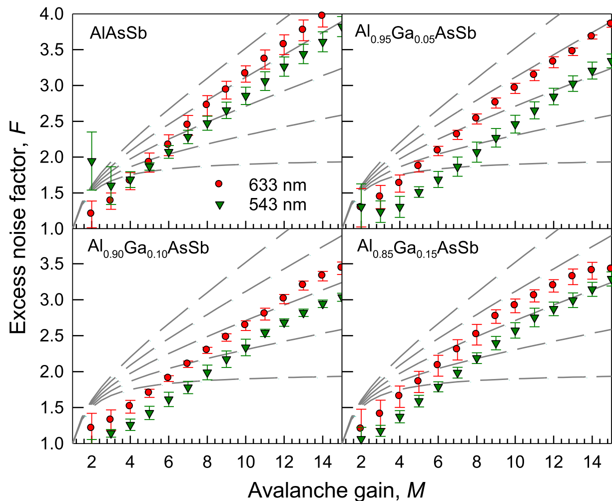

Fig. 4. Excess noise factor versus avalanche gain characteristics measured with laser wavelengths 633nm (•) and 543nm (▼), from AlAsSb, $Al_{0.95}Ga_{0.05}AsSb$, $Al_{0.90}Ga_{0.10}AsSb$, and $Al_{0.85}Ga_{0.15}AsSb$ diodes. The grey dashed lines are calculated using McIntyre's local model [1] for *k* from 0 to 0.2 in steps of 0.05.

the *i*-layer and fewer holes injected from the n^+ layer. This suggests that, in the $Al_{1-x}Ga_xAs_{0.56}Sb_{0.44}$ ($x = 0$ to 0.15), the electron ionization coefficient is higher than the hole ionization coefficient, i.e. $\alpha > \beta$.

Fig. 4 shows the experimental mean and standard deviation of *F*(*M*) from the four wafers. Lines of *F*(*M*) based on the classical McIntyre model [1] for effective $k = 0$ to 0.20 in steps of 0.05 are included for reference. In all the wafers, *F*(*M*) characteristics improve (decreases) when the laser wavelength decreases. This again suggests that $\alpha > \beta$ in the $Al_{1-x}Ga_xAs_{0.56}Sb_{0.44}$ alloy used in this work. The lowest *F*(*M*) characteristics measured in these devices correspond to the effective $k = 0.1$ lines. In AlAsSb, the lowest excess noise was measured under pure electron injection, achieved using a UV laser [15]. Therefore we believe that using a shorter wavelength laser to achieve a pure electron injection profile is likely to yield even lower excess noise characteristics in these $Al_{1-x}Ga_xAs_{0.56}Sb_{0.44}$ ($x = 0$ to 0.15) alloys.

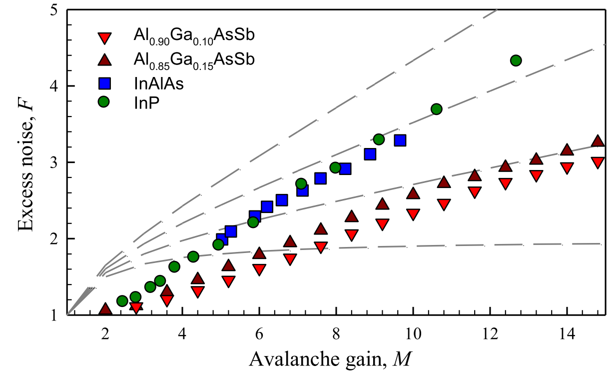

Fig. 5. Comparison of excess noise versus gain characteristics of $Al_{0.85}Ga_{0.15}AsSb$ $w = 100$ nm diode, InP $w = 250$ nm diode [26], and InAlAs $w = 100$ nm diode [27]. The dashed lines are calculated using McIntyre's local model of *k* from 0 to 0.3 in steps of 0.1.

The excess noise characteristics of these $Al_{1-x}Ga_xAs_{0.56}Sb_{0.44}$ ($x = 0.10$ to 0.15) APDs obtained using 543 nm wavelength laser are compared with previous reports of InP and InAlAs diodes in Fig. 5. The data from alloys with $x = 0$ and $x = 0.05$ are excluded due to their highly mixed carrier injection profiles. The InP [26] and InAlAs [27] data chosen for this comparison were from experiments that used the preferred carrier injection conditions, i.e pure hole injection for InP and pure electron injection for InAlAs. The values of *w* of the InP and InAlAs diodes are 250 and 100 nm, respectively. There is no available data for InP diode with *w* ~100 nm. Lower excess noise was clearly observed in our $Al_{1-x}Ga_xAs_{0.56}Sb_{0.44}$ ($x = 0.10$ to 0.15) diodes despite not achieving pure electron injection.

When compared to excess noise measured under pure electron injection in an 80 nm AlAsSb avalanche region [15], our measured excess noise is also marginally lower. Our results suggests that under pure electron injection conditions, the excess noise performance in $Al_{1-x}Ga_xAs_{0.56}Sb_{0.44}$ ($x = 0.05$ to 0.15) APDs with a thin (110–116 nm avalanche region may approach the lowest noise reported in a 230 nm AlAsSb avalanche layer. Unlike thin layers of InP and InAlAs, that suffer from high tunneling current [16], we demonstrated that thin (110-116 nm) AlGaAsSb avalanche layers can produce very low excess noise without exhibiting excessive band to band tunneling currents. Therefore they can be excellent candidates for the avalanche layer in high speed APDs for high bit rate optical communication systems.

IV. Conclusion

In this paper, the avalanche gain and excess noise characteristics of thin $Al_{1-x}Ga_xAsSb$ (x = 0 to 0.15) avalanche layers have been presented. Avalanche gain and excess noise measurements performed on $Al_{1-x}Ga_xAsSb$ diodes with avalanche layers of 110–116 nm thick indicate that the electron ionization coefficient is higher than the hole ionization coefficient. The lowest excess noise measured, corresponding to an effective k

of 0.1, were from $Al_{1-x}Ga_xAs_{0.56}Sb_{0.44}$ (x = 0.05 to 0.15) under mixed injection condition. These are much lower than the reported data for InP and InAlAs. Therefore high gain and low excess noise can be obtained in thin $Al_{1-x}Ga_xAs_{0.56}Sb_{0.44}$ without suffering from excessive band to band tunneling current.

References

[1] R. J. McIntyre, "Multiplication noise in uniform avalanche diodes," *IEEE Trans. Electron Devices*, vol. ED-13, no. 1, pp. 164–168, Jan. 1966.

[2] R. B. Emmons, "Avalanche-photodiode frequency response," *J. Appl. Phys.*, vol. 38, no. 9, pp. 3705–3714, Aug. 1967.

[3] K. F. Li *et al.*, "Avalanche multiplication noise characteristics in thin GaAs p+ -i-n+ diodes," *IEEE Trans. Electron Devices*, vol. 45, no. 10, pp. 2102–2109, Oct. 1998.

[4] P. Yuan *et al.*, "Impact ionization characteristics of III-V semiconductors for a wide range of multiplication region thicknesses," *IEEE J. Quantum Electron.*, vol. 36, no. 2, pp. 198–204, Feb. 2000.

[5] M. M. Hayat, B. A. E. Saleh, and M. C. Teich, "Effect of dead space on gain and noise of double-carrier-multiplication avalanche photodiodes," *IEEE Trans. Electron Devices*, vol. 39, no. 3, pp. 546–552, Mar. 1992.

[6] D. S. Ong *et al.*, "Monte Carlo estimation of avalanche noise in thin p+-i-n+ GaAs diodes," *Appl. Phys. Lett.*, vol. 72, no. 2, pp. 232–234, Jan. 1998.

[7] D. S. G. Ong, M. M. Hayat, J. P. R. David, and J. S. Ng, "Sensitivity of high-speed lightwave system receivers using InAlAs avalanche photodiodes," *IEEE Photon. Technol. Lett.*, vol. 23, no. 4, pp. 233–235, Feb. 2011.

[8] K. S. Hyun, Y.-H. Kwon, and I. Yun, "Characteristics of a planar InP/InGaAs avalanche photodiode with a thin multiplication layer," *J. Korean Phys. Soc.*, vol. 44, no. 4, pp. L779–L784, Apr. 2004.

[9] S. Hwang, J. Shim, and K. Yoo, "A 10-Gb/s planar InGaAs/InP avalanche photodiode with a thin multiplication layer fabricated by using recess etching and single-diffusion processes," *J. Korean Phys. Soc.*, vol. 49, no. 1, pp. 253–260, Jul. 2006.

[10] M. Nada, H. Yokoyama, Y. Muramoto, T. Ishibashi, and H. Matsuzaki, "A 50-Gbit/s vertical illumination avalanche photodiode for 400-Gbit/s Ethernet systems," *Opt. Express*, vol. 22, no. 12, Jun. 2014, Art. no. 14681.

[11] M. Lahrichi *et al.*, "240-GHz gain-bandwidth product back-side illuminated AlInAs avalanche photodiodes," *IEEE Photon. Technol. Lett.*, vol. 22, no. 18, pp. 1373–1376, 2010.

[12] Y. M. Kang *et al.*, "Monolithic germanium/silicon avalanche photodiodes with 340 GHz gain-bandwidth product," *Nature Photon.*, vol. 3, pp. 59–63, Jan. 2009.

[13] M. Ren *et al.*, "Characteristics of $Al_xIn_{1-x}As_ySb_{1-y}$ (x:0.3-0.7) avalanche photodiodes," *J. Lightw. Technol*, vol. 35, no. 12, pp. 2380–2384, Jun. 2017.

[14] S. Xie and C. H. Tan, "AlAsSb avalanche photodiodes with a sub-mV/K temperature coefficient of breakdown voltage," *IEEE J. Quantum Electron.*, vol. 47, no. 11, pp. 1391–1395, Nov. 2011.

[15] J. Xie, S. Xie, R. C. Tozer, and C. H. Tan, "Excess noise characteristics of thin AlAsSb APDs," *IEEE Trans. Electron Devices*, vol. 59, no. 5, pp. 1475–1479, May 2012.

[16] X. Zhou, S. Zhang, J. P. R. David, J. S. Ng, and C. H. Tan, "Avalanche breakdown characteristics of $Al_{1-x}Ga_xAs_{0.56}Sb_{0.44}$ quaternary alloys," *IEEE Photon. Technol. Lett.*, vol. 28, no. 22, pp. 2495–2498, Nov. 2016.

[17] S. Xie *et al.*, "InGaAs/AlGaAsSb avalanche photodiode with high gain-bandwidth product," *Opt. Express*, vol. 24, pp. 24242–24247, 2016.

[18] M. H. Woods, W. C. Johnson, and M. A. Lampert, "Use of Schottky barrier to measure impact ionization coefficients in semiconductors," *Solid-State Electron.*, vol. 16, no. 3, pp. 381–394, 1973.

[19] F. R. Bacher, J. S. Blakemore, J. T. Ebner, and J. R. Arthur, "Optical-absorption coefficient of $In_{1-xG}a_xAs$/InP," *Phys. Rev. B*, vol. 37, no. 5, pp. 2551–2557, 1988.

[20] N. Georgiev and T. Mozume, "Photoluminescence study of InGaAs/AlAsSb heterostructure," *J. Appl. Phys.*, vol. 89, no. 2, pp. 1064–1069, Jan. 2001.

[21] Y. Nakata *et al.*, "InGaAs/AlAsSb heterostructures lattice-matched to InP grown by molecular beam epitaxy," in *Mat. Res. Soc. Symp. Proc.*, vol. 198, pp. 289–294, 1990.

[22] M. R. Lorenz, R. Chicotka, G. D. Pettit, and P. J. Dean, "The fundamental absorption edge of AlAs and AlP," *Solid State Commun.*, vol. 8, no. 9, pp. 693–697, 1970.

[23] S. Zollner, C. Lin, E. Schönherr, A. Böhringer, and M. Cardona, "The dielectric function of AlSb from 1.4 to 5.8 eV determined by spectroscopic ellipsometry," *J. Appl. Phys.*, vol. 66, no. 1, pp. 383–387, Jul. 1989.

[24] S. Adachi, "Optical dispersion relations for GaP, GaAs, GaSb, InP, InAs, InSb, $Al_xGa_{1-x}As$, and $In_{1-x}Ga_xAs_yP_{1-y}$," *J. Appl. Phys.*, vol. 66, no. 12, pp. 6030–6040, Dec. 1989.

[25] X. Zhou *et al.*, "Thin $Al_{1-x}Ga_xAs_{0.56}Sb_{0.44}$ diodes with extremely weak temperature dependence of avalanche breakdown," *Roy. Soc. Open Sci.*, vol. 4, no. 5, May 2017, Art. no. 170071.

[26] L. J. J. Tan, J. S. Ng, C. H. Tan, and J. P. R. David, "Avalanche noise characteristics in submicron InP diodes," *IEEE J. Quantum Electron.*, vol. 44, no. 4, pp. 378–382, Apr. 2008.

[27] Y. L. Goh *et al.*, "Excess avalanche noise in $In_{0.52}Al_{0.48}As$," *IEEE J. Quantum Electron.*, vol. 43, no. 6, pp. 503–507, Jun. 2007.

Xinxin Zhou received the M.Sc. and Ph.D. degrees in electronic engineering from the University of Sheffield, Sheffield, U.K., in 2010 and 2014, respectively. From 2014 to 2017, she was a Research Associate in the Department of Electronic and Electrical Engineering, University of Sheffield, and was responsible for fabrication and characterization of high sensitivity midinfrared detectors and high-speed avalanche photodiodes. She has recently become a Senior Product Engineer of Detectors in Oclaro Technology, Ltd., Towcester, U.K.

Lucas L. G. Pinel received a double M.Sc.Eng. degree in physics and nanosciences from Grenoble Institute of Technology, Grenoble, France, and in engineering physics from the Royal Institute of Technology, Stockholm, Sweden, in 2015.

He is currently working toward the Ph.D. degree in electronic and electrical engineering at the University of Sheffield, Sheffield, U.K., focusing his doctoral research on avalanche photodiodes for X-ray detection.

Simon J. Dimler received the M.Eng. and Ph.D. degrees in electronic and electrical engineering from the University of Sheffield, Sheffield, U.K.

His current research interest focuses on development of single photon detectors and instrumentation for the characterization of photodetectors.

Shiyong Zhang received the B.S. degree in material science from Tsinghua University, Beijing, China, in 2000 and the Ph.D. degree in microelectronics and solid-state electronics from the Chinese Academy of Sciences, Beijing, China, in 2006, respectively. Since 2006, he has been with the National Centre for III–V Technologies, Engineering and Physical Sciences Research Council, Sheffield, U.K., and responsible for molecular- beam epitaxy growth of antimony-containing structures. His research interests include quantum cascade lasers, infrared photodetectors, and high mobility two-dimensional electron gases.

Jo Shien Ng (M'99) received the B.Eng. and Ph.D. degrees in electronic engineering from the University of Sheffield, Sheffield, U.K., in 1999 and 2003, respectively.

She is currently a Professor of semiconductor devices in the Department of Electronic and Electrical Engineering, University of Sheffield. She was a Royal Society Research Fellow based in the same department between 2006 and 2016. Her research interests include avalanche photodiodes, Geiger-mode avalanche photodiodes, and material characterization.

Chee Hing Tan (M'95) received the B.Eng. and Ph.D. degrees in electronic engineering from the Department of Electronic and Electrical Engineering, University of Sheffield, Sheffield, U.K., in 1998 and 2002, respectively.

He is currently a Professor of opto-electronic sensors in the Department of Electronic and Electrical Engineering, University of Sheffield. He has extensive experience in the characterization and modeling of high-speed low-noise avalanche photodiodes and phototransistors. His current research interests include single-photon avalanche diodes, midinfrared photodiodes, quantum-dot infrared detectors, X-ray detectors, ultrahigh-speed avalanche photodiodes, and phototransistors.